Morphology of Thermoplastic Elastomers: Elastomeric Polypropylene

Holger Schönherr,[†,‡,#] Willy Wiyatno,[†,‡] John Pople,[†,‡,§] Curtis W. Frank,[*,†,‡] Gerald G. Fuller,[†,‡] Alice P. Gast,[†,‡,§] and Robert M. Waymouth[*,†,⊥]

Department of Chemical Engineering, Stanford University, Stanford, California 94305-5025; NSF MRSEC Center on Polymer Interfaces and Macromolecular Assemblies (CPIMA); Stanford Synchrotron Radiation Laboratory, Stanford Linear Accelerator Center, Stanford University, Stanford, California 94309; and Department of Chemistry, Stanford University, Stanford, California 94305-5080

Received June 1, 2001; Revised Manuscript Received December 27, 2001

ABSTRACT: The morphology of low-density (0.86 g/cm^3), low-crystallinity (10%) elastomeric polypropylene (ePP) derived from a bis(2-arylindenyl)hafnium catalyst was investigated using a combination of polarized optical microscopy (POM), differential scanning calorimetry (DSC), wide-angle X-ray scattering (WAXS), Fourier transform infrared (FT-IR) spectroscopy, and tapping mode atomic force microscopy (TM-AFM). This thermoplastic elastomer, when crystallized isothermally from the melt, exhibits morphologies reminiscent of classical semicrystalline polymers. The presence of lamellae, crosshatching, hedrites, and spherulites was revealed by high-resolution TM-AFM. POM confirmed the presence of hedrites and spherulites. The parent ePP can be fractionated into components of different average tacticities ([mmmm]%: 21%−76%) and crystallinities (1%−40% as determined by DSC and WAXS) but more similar molecular mass (M_w: 147−432 kg/mol) and polydispersity (M_w/M_n: 2.1−2.5). The analysis of the morphologies of these fractions revealed large hierarchical structures for all but the lowest crystallinity fraction and crosshatching typical of the α-modification of crystalline isotactic polypropylene for all fractions. The solubility of the corresponding fractions in ether and heptane combined with new evidence for crystals with melting temperatures higher than 100 °C in all of the fractions is most consistent with a stereoblock microstructure of atactic and isotactic sequences in ePP.

Introduction

Many recent advances in polymer materials science have been triggered by the development of improved synthetic methods, including the creation of single-site catalysts for controlled polymerizations,[1−3] novel polymerization techniques,[4,5] and highly specific polymerizations using cloning strategies.[6] These new synthetic techniques are providing higher levels of control over composition, molecular mass distributions, branching, and stereoregularity.[1] As a consequence, a wide variety of polymers with unusual properties can be designed and synthesized. For instance, while thermoplastic elastomers based on polypropylene have been known since the 1950s,[7] new catalysts and synthetic strategies have led to new classes of these materials and fresh insights into the origin of their elastomeric properties.[8−10] Polymers synthesized using heterogeneous Ziegler−Natta catalysts have rather broad molecular mass and tacticity distributions;[7,8a,b] by contrast, homogeneous metallocene catalysts produce a much more narrowly distributed polymer.[9,11] Elastomeric polypropylenes derived from unbridged bis(2-arylindenyl) metallocenes are intermediate and can be fractionated into components of different tacticity and crystallinity but similar molar mass and polydispersity.[10,12] The structure and properties of elastomeric polypropylenes (ePP) derived from bis(2-arylindene) metallocenes[10] have been the subject of study by a variety of techniques.[12,13]

These polypropylene materials are members[14−16] of the class of thermoplastic elastomers since they possess the physical properties of elastomers and the processing characteristics of thermoplastics.[16] These materials are characterized by a low degree of crystallinity,[12a,b,17] where the crystalline regions dispersed in the amorphous matrix are thought to provide physical cross-links for the amorphous elastomeric segments of the chain.[7] The size and distribution of these crystalline regions in the amorphous matrix should have important influences on the mechanical properties. It is therefore of particular interest to analyze and understand how, and to what extent, these polyolefin elastomers crystallize and how the material properties are related to the underlying semicrystalline morphology.

Little is known of the morphology of low-crystallinity, elastomeric polypropylenes. Kravchenko and co-workers recently used tapping-mode atomic force microscopy (TM-AFM) to image the morphology of metallocene ePP and the changes in surface morphology resulting from tensile extension experiments.[13] On the basis of their TM-AFM images, these authors showed that the unstrained ePP crystallizes in the form of individual short lamellae embedded in an amorphous matrix. This morphology, which was attributed to the much lower crystallinity of the elastomeric polypropylene, is markedly different from the morphology found by AFM and other techniques for isotactic polypropylene (iPP) in either the α- or β-modifications.[18−22]

The morphology of low-crystallinity polyethylene-based thermoplastic elastomers has been studied by

† Department of Chemical Engineering, Stanford University.
‡ CPIMA.
§ Stanford Linear Accelerator Center, Stanford University.
⊥ Department of Chemistry, Stanford University.
Present address: University of Twente, Faculty of Chemical Technology and MESA Research Institute, Department of Materials Science and Technology of Polymers, P.O. Box 217, 7500 AE Enschede, The Netherlands.
* Corresponding authors. C.W.F.: phone: 650 723-9780; FAX 650 723-4573; e-mail curt@chemeng.stanford.edu. R.M.W.: phone 650 723-4515; FAX 650 725-0259; e-mail waymouth@leland.stanford.edu.

10.1021/ma010959m CCC: $22.00
Published on Web 03/01/2002

Table 1. Polymer Characterization

sample	wt %	M_w (10^3)[a]	M_w/M_n[a]	[mmmm] (%)[b]	[m] (%)[c]
ePP-10	100	201	2.3	34	73
ES-ePP10	48	147	2.1	21	67
HS-ePP10	42	220	2.3	44	79
HI-ePP10	10	432	2.5	76	92

[a] Determined by high-temperature GPC at BP Amoco Chemical Co. [b] Determined by ^{13}C NMR, the fraction of five contiguous isotactic stereosequences in the polymer. [c] Determined by ^{13}C NMR, the fraction of isotactic dyads in the polymer.

Bensason et al.[15] These authors showed that the physical properties of these low-density polyethylenes correlated with the amount of comonomer, density, crystallinity, and morphology. At high crystallinities, spherulitic morphologies were observed, and at intermediate crystallinities the polyethylenes adopted a stacked lamellar morphology. For polyethylenes with densities less than 0.89 g/cm^3, a granular morphology was observed and proposed to be made up of bundled crystals or fringed micelles. The transition from lamellar morphology to the granular "fringed micelle" coincided with the onset of elastomeric properties.

In this contribution, we detail our investigations of the morphology and crystallinity of ePP synthesized with a bis(2-arylindenyl)hafnium dichloride catalyst as well as several of the fractions. The compositional heterogeneity of these materials has allowed us to study the crystallinity, morphology, and thermal properties as a function of stereoregularity. We show that ePP can crystallize with morphology reminiscent of much more highly crystalline polypropylenes. In particular, we show that polypropylenes with densities as low as 0.86 g/cm^3 and their fractions are crystalline with lamellar and crosshatched lamellar morphology, which organize into hedrites or spherulites, depending on the overall crystallinity and thermal history. The observed morphology has consequences for the mechanical properties of these thermoplastic elastomeric materials, which will be described elsewhere.[23]

Experimental Section

Materials. The elastomeric polypropylene (ePP) was synthesized by BP Amoco Chemical Co. (ePP-10) in liquid propylene at 50 °C using bis(2-(3,5-di-*tert*-butylphenyl)indenyl)-hafnium dichloride as catalyst.[24] Fractionation was carried out by successive solvent extraction of ePP with boiling diethyl ether and heptane under a nitrogen environment following the procedure reported previously.[12] Three fractions with an increasing isotacticity were obtained: ether-soluble (ES, lowest isotacticity), heptane-soluble (HS, medium isotacticity), and heptane-insoluble (HI, highest isotacticity) (see Table 1). Table 1 shows the characterization data of the elastomeric polypropylene ePP together with its fractions.[24] The original ePP-10 may contain catalyst residues, but the ES, HS, and HI materials are unlikely to contain such residues due to the exhaustive fractionation.

Sample Preparation. All samples investigated were initially melt-pressed between two protective Teflon sheets (Mechanical Grade PTFE, McMaster-CARR) at 180 °C[25] under a pressure of 500 psi in a hot-press (model C, Carver, Menomonee Falls, WI). The film samples obtained had a typical thickness of ca. 0.5 mm. Subsequently, samples were melted at 180 °C in a custom-built hot stage (based on a model PC-600 hot stage, Corning, Acton, MA) equipped with a temperature controller (CSS-8094 Omega, Stamford, CT) in an argon atmosphere. After melting, either the samples were cooled to room temperature with a typical rate of 5 °C (nonisothermal crystallization) or they were crystallized isothermally (e.g., at 120 °C) for 6 h and quenched with liquid nitrogen. To ensure a consistent thermal history for both isothermal and nonisothermal crystallization, all samples of a given thermal history were prepared simultaneously.

For the AFM and FT-IR experiments, films supported on silicon wafers were used. For this purpose, melt-pressed samples (vide supra) were transferred onto precleaned silicon wafers and melted with uncovered free surfaces at 180 °C in argon. These films are referred to as bulk films with thickness of about 0.5 mm. Thin films were also prepared by spin-coating a solution of ePP in xylenes at high temperatures directly onto a precleaned silicon wafer followed by drying in vacuo at 25 °C for several days.[26] For the optical microscopy study, samples placed on microscope slides (with cover slides) were melt-pressed to a thickness of around 50 μm before being thermally treated.

Tapping Mode AFM (TM-AFM). The TM-AFM data were acquired in an ambient atmosphere (30%−40% humidity, 24 °C temperature[27]) with a NanoScope III multimode AFM (Digital Instruments (DI), Santa Barbara, CA) using microfabricated silicon tips/cantilevers (Nanosensors, Wetzlar, Germany).[28] For imaging at elevated temperatures a custom-built hot stage was used.[29] Height (constant amplitude damping), amplitude, and phase images were recorded simultaneously at multiple locations on at least two specimens. While the height images show the profile of the sample surface quantitatively (assuming that the oscillation of the cantilever is damped similarly at all locations), the amplitude and phase images provide in some cases much clearer contrast of the features imaged compared to height images. Here the contrast depends on various imaging conditions such that no *z*-scale is provided in the figure captions. In the amplitude images the outlines of topographical features, such as radiating fibrillar structures, are seen. The adjusted set point ratio of ca. 0.7 to 0.8 results in a stiffness-dominated contrast in the phase images, which allowed us to differentiate between stiff crystalline features and the less-stiff amorphous phase in the near-surface region of the films.[30,31] The images shown here were subjected to a first-order plane-fitting procedure to compensate for sample tilt. Using the "bearing analysis" (DI NanoScope software), which is a quantitative analysis of the distribution of depths present in the image, we assessed the crystallinity in a semiquantitative manner. This crude estimate was based on the assumption that bright contrast in the TM-AFM phase images corresponds exclusively to the crystalline phase, whereas dark contrast corresponds to the amorphous phase. Images in flat regions with pronounced crosshatching (except for ES where these were scarce) were chosen for this analysis.

Polarized Optical Microscopy (POM). The optical light microscopy investigations were carried out with an optical microscope (Axioplan D-7082, Zeiss) in transmission mode with crossed polarizers. A digital camera (Hamamatsu C4742-95) connected to a personal computer was used to capture the optical microscopy images.

Differential Scanning Calorimetry (DSC). Thermal analysis was performed on a Perkin-Elmer 7 differential scanning calorimeter using indium as calibration standard. Melt-pressed polymers with a thickness of about 0.1 mm were frozen in liquid N_2 and punched cut with a standard single-hole paper puncher. Disklike samples of 5−15 mg were weighed and sealed into Perkin-Elmer aluminum DSC pans. The thermal treatment of DSC samples was carried out in the DSC instrument under a N_2 atmosphere. All samples were initially preheated to 200 °C with a rate of 40 °C/min and held at 200 °C for 5 min. For the nonisothermal thermal history, samples were cooled from 200 °C to room temperature at 20 °C/min. The isothermal samples were cooled from 200 to 120 °C at 20 °C/min and annealed for 6 h. After annealing, samples were cooled to room temperature using the same cooling rate. All samples were aged for at least 20 h at room temperature. After aging, samples were cooled to −25 °C at 20 °C/min and held for 5 min before endotherm scans were carried out. Melting points (T_m) (peak of endotherm curve) and heat of fusion (ΔH_f) were measured by heating from −25 to 200 °C with a rate of 20 °C/min. The crystallinity was calculated by

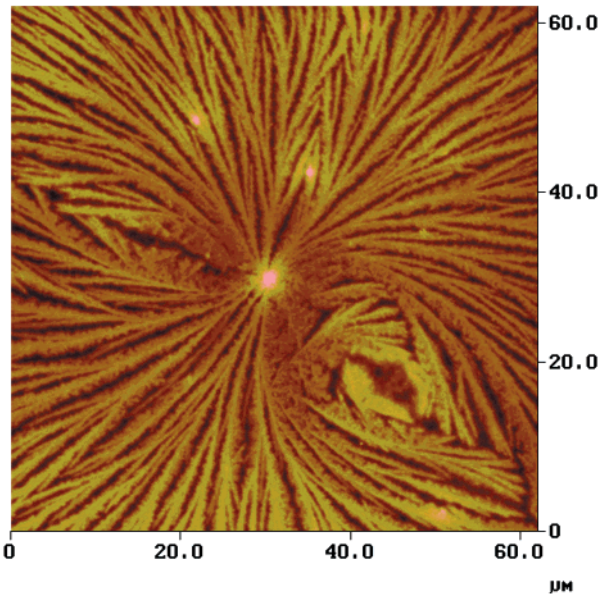

Figure 1. TM-AFM height images of unfractionated ePP crystallized isothermally at 130 °C in a 200 nm thin film on oxidized Si (*z* scale from dark to bright 200 nm).

normalizing the heat of fusion (ΔH_f) from the endotherm scans by the theoretical value of a completely crystalline sample of 209 J/g.[32]

Wide-Angle X-ray Scattering (WAXS). WAXS experiments were performed at the Stanford Linear Accelerator Center (SLAC) on beamline 1-4 of the Stanford Synchrotron Radiation Laboratory (SSRL). The X-ray source is focused with a flux ~10^{10} photons and monochromated by a (111) Si crystal to a wavelength of $\lambda = 1.488$ Å. A CCD-based area detector (Photonic Science) with a 1024 × 1024 array of 25 μm square pixels was used to collect the 2-D diffraction data image. Images were assembled from the summation of 1000 consecutive scans, and the portion of reciprocal space imaged was calibrated with a Lupolen standard. Data analysis was performed using 1-D profiles summed radially from the 2-D patterns and corrected for background scattering and scattering from windows associated with the optics. The scattering intensities are presented as a function of scattering vector q, which is defined as $q = [4\pi \sin(\theta/2)]/\lambda$.

Fourier Transform Infrared Spectroscopy (FT-IR). The FT-IR data were obtained on thin films on a BIO-RAD FTS-60A FT-IR spectrometer operated in transmission mode. A total of 64−128 scans were collected with a resolution of 2 cm^{-1} and ratioed against the previously collected background spectrum. The band at 998 cm^{-1} corresponds to a helical conformation of a sequence of approximately 10−14 isotactic repeat units, whereas the 975 cm^{-1} band corresponds to head-to-tail sequences of propylene units.[33] The absorbances of the bands at ca. 998 cm^{-1} and ca. 975 cm^{-1} were integrated using the peak fitting procedures of the BIO-RAD WIN-IR Pro software. The ratio of these two bands was previously shown to be nearly linearly dependent on the crystallinity of iPP.[34]

Results

The morphology of melt-crystallized films of the unfractionated ePP was investigated first by tapping-mode atomic force microscopy (TM-AFM). As shown in Figure 1, a 200 nm thin film of unfractionated ePP crystallized for 6 h at 130 °C formed giant two-dimensional spherulites. From this low-magnification AFM micrograph, the preferred initial growth direction, the branching and splaying of stacks of lamellae under small angles, and the filling of the space in the eyes or so-called Popoff's leaves can be clearly seen.[35] The final attainment of the disklike envelope of this specimen was verified in sequentially recorded AFM images.[36] This image corresponds very well to images obtained by various microscopic techniques on classical semicrystalline polymers and agrees with the established view of how typical polymer spherulites develop by nucleation and growth.[37]

Similar morphologies were found at the surface of bulk films of unfractionated ePP. Intermediate stages of development of spherulitic growth, so-called hedrites,[38] are evident in Figure 2 together with a higher magnification micrograph of regions next to the hedrites, which shows edge-on lamellae and a dense crosshatching pattern. The observation of a crosshatched morphology with branching at crystallographi-

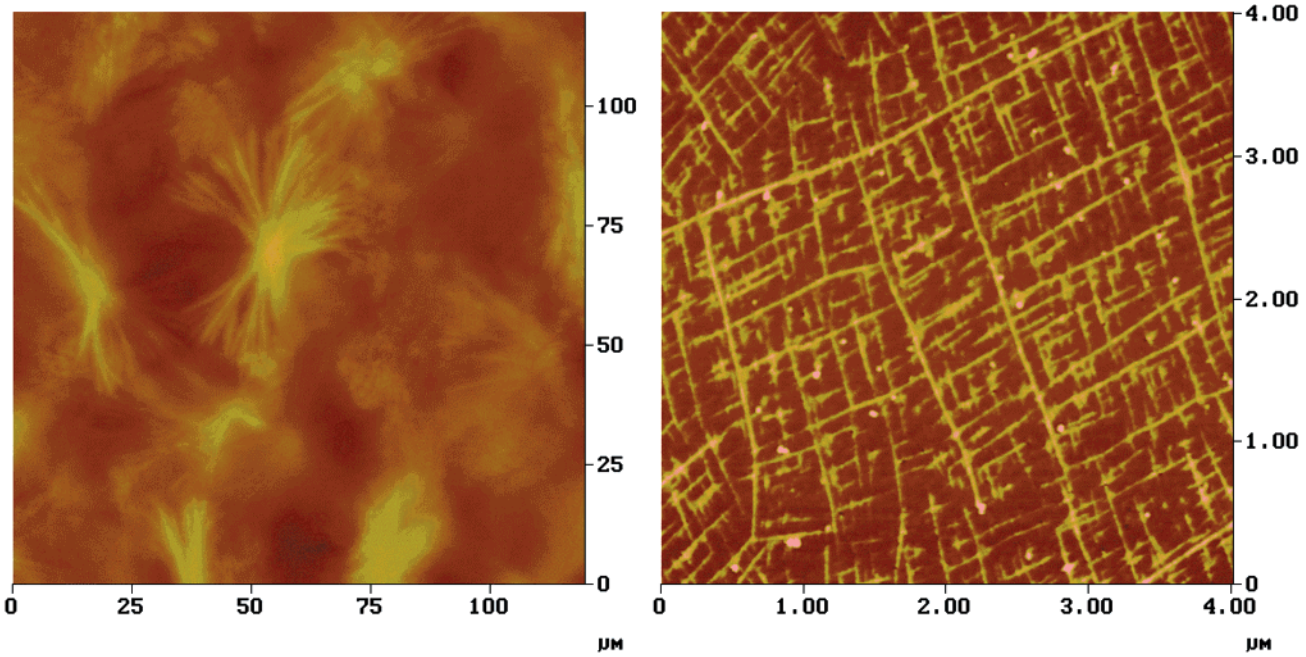

Figure 2. TM-AFM images of unfractionated ePP bulk film crystallized isothermally at 120 °C (left: height image, *z* scale from dark to bright 3.5 μm; right: phase image).[57]

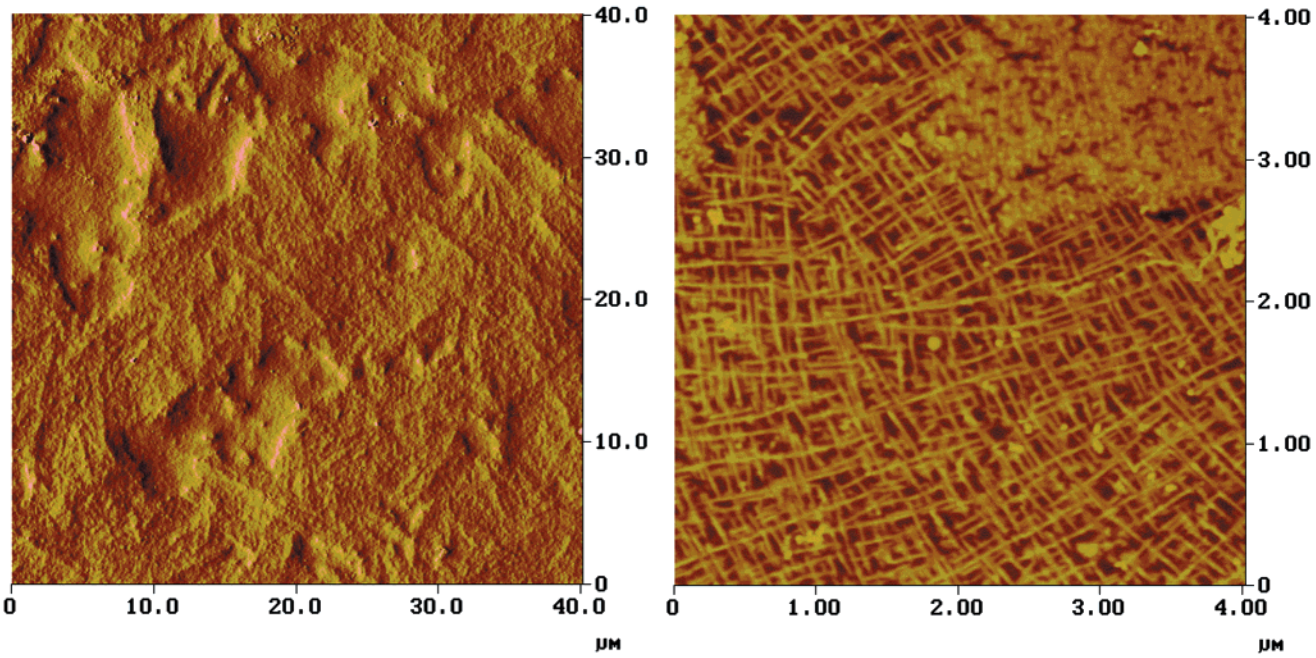

Figure 3. TM-AFM images of unfractionated ePP bulk film crystallized nonisothermally (left, amplitude image; right, phase image).[57]

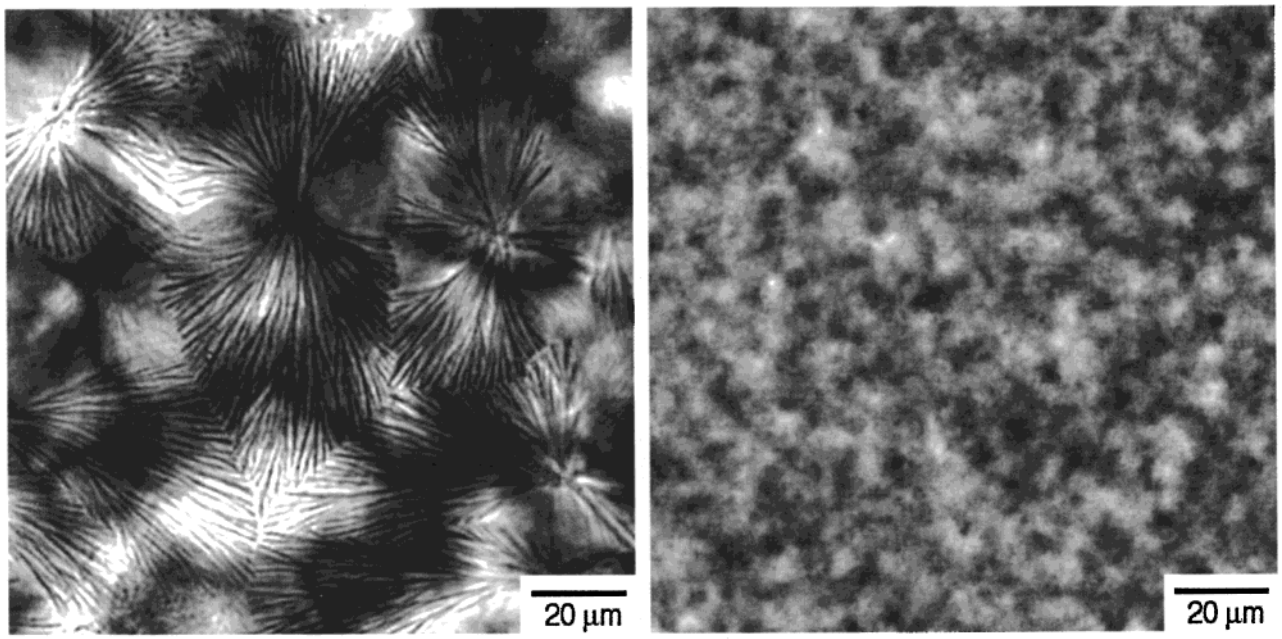

Figure 4. Optical micrographs obtained with crossed polarizers on unfractionated ePP films crystallized isothermally at 120 °C (left) and nonisothermally (right).

cally defined angles in these ePP samples is evidence for the presence of the monoclinic α-modification of iPP.[39] The angle measured between lamellae and their branches for the ePP specimens was 80 ± 2°, which compares favorably with the theoretically predicted and experimentally observed angle of 80.4°.[39c] The observation of thick dominant lamellae, branching with a defined angle of 80°, and thin branches agrees well with the results of previous morphological studies on iPP.[35,40] The large-scale organization in the nonisothermally crystallized film (Figure 3) is less perfect, and the observed features are smaller; however, the presence of crosshatching can be noted as well.

From cross-sectional plots we estimate average (convoluted) thicknesses of the crystalline features of 20 ± 3, 23 ± 4, and 28 ± 6 nm for ePP crystallized isothermally at 110, 120, and 130 °C, respectively. A quantitative determination of the thicknesses of these features from high-resolution AFM images is inaccurate due to tip convolution. On the basis of imaging of a calibration standard,[41] the radii of the tips used in our studies were estimated to be 5−15 nm. A quantitative deconvolution of the AFM images, however, was not attempted due to the uncertainty on the penetration depth and the geometry of the experiment; i.e., it is not a priori clear whether and to what extent these features protrude from the surface. While the thickness measured for these features are larger than what we expect for lamellae that melt at these melting temperatures, a comparison of these values with lamellar thicknesses

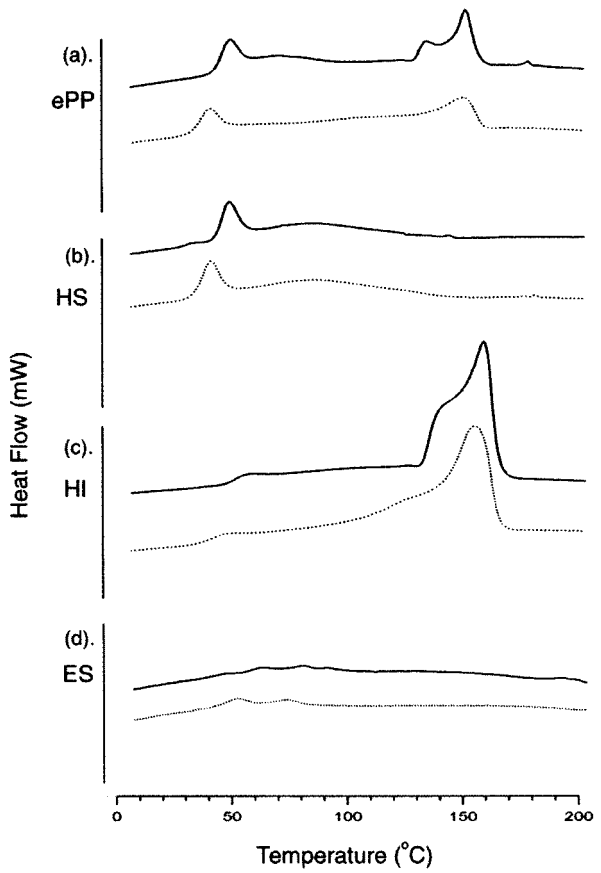

Figure 5. Differential scanning calorimetry (DSC) endotherm scans of isothermally crystallized (120 °C, solid curves) and nonisothermally crystallized samples (dotted curves) of (a) unfractionated ePP, (b) HS fraction, (c) HI fraction, and (d) ES fraction. Curves are shifted along the *y*-axis for clarity.

reported for iPP in the literature[42] indicates that we have resolved individual edge-on lamellae.

Bulk morphology of ePP was also investigated by optical microscopy with crossed polarizers to complement the AFM technique (Figure 4). A typical POM image of unfractionated ePP crystallized isothermally at 120 °C (left) and crystallized nonisothermally (right) reveals birefringent spherulitic and hedritic features for the former. A Maltese cross extinction pattern is not observed due to the limited size and imperfection of the hedrites and spherulites. In these experiments the focal plane was changed systematically in order to ensure that the observed features are not segregated crystallites at the film−air interface. The nonisothermally crystallized samples show little birefringence and no discernible morphological features, which is consistent with more disordered crystallites seen by TM-AFM. These POM results indicate that the morphologies observed by TM-AFM at the free surface of the samples are representative for the whole volume of the film.

Thermal analysis of isothermally (120 °C for 6 h) and nonisothermally crystallized samples was carried out for ePP and for each fraction by DSC (Figure 5). The nonisothermally crystallized ePP shows a broad melting transition with two dominant peaks centered at 42 and 149 °C. Isothermal crystallization results in a shift of the melting peaks to 50 and 150 °C, respectively, and the appearance of another melting peak at 135 °C. For the HS fraction, there was only one dominant peak centered at 42 °C, which was shifted to 50 °C upon

Table 2. Effect of Isothermal Crystallization.

			crystallinity	
sample	T_m (°C)[a]	ΔH_f (J/g)[a,b]	DSC[a] (%)	WAXS (%)
ePP nonisothermal	42−149	22	11 ± 1	8 ± 2
ePP isothermal	50−150	22	11 ± 1	9 ± 2
ES nonisothermal	41−45	2	1 ± 1	1 ± 1
ES isothermal	41−45	2	1 ± 1	1 ± 1
HS nonisothermal	42	32	15 ± 2	11 ± 2
HS isothermal	50	32	15 ± 2	14 ± 2
HI nonisothermal	47−155	82	39 ± 2	37 ± 2
HI isothermal	57−158	83	40 ± 2	41 ± 2

[a] Determined by DSC, endotherm scan from −20 to 200 °C at 20 °C/min. [b] Standard deviation of ΔH_f is ±2 J/g.

isothermal crystallization. It is clear that the majority of the material of the HS fraction must have crystallized during or after cooling. The HI fraction had a broad melting range with the first peak at 47 °C, extending up to another peak at 155 °C. After isothermal crystallization, the lower temperature melting peak was shifted to 57 °C and the higher temperature melting peak (shifted to 158 °C) became more pronounced with an additional melting shoulder at around 142 °C. The ES fraction showed only barely measurable endotherms in the DSC thermal analysis. The crystallinities determined by DSC and WAXS are summarized in Table 2.

Wide-angle X-ray scattering experiments were performed to study the effect of thermal history on the crystallinity. Isothermal crystallization conditions (120 °C for 6 h) were contrasted with nonisothermal crystallization conditions (Figure 6). The crystalline peaks in the WAXS scattering plots of the unfractionated ePP and the HS and HI fractions are due to the α-phase of iPP, namely the reflections of the (110), (040), (130), (111), and (−131) planes.[18] No clear signature of the γ-phase of iPP was found. The positions of the observed scattering peaks are listed in Table 3 together with the corresponding *d*-spacings. The lowest isotacticity fraction (ES) exhibits a faint scattering peak that could indicate the presence of either a smectic or β phase,[12,43] but the data do not allow a definitive assignment.

The percent crystallinity was calculated from the ratio of the area of the corresponding peaks (after subtraction of the amorphous halo measured using an atactic polypropylene sample measured at 25 °C)[44] to the total area under the curves. The crystallinity of each fraction as measured by WAXS is in good agreement with the crystallinity measured by DSC (Table 2). As shown in Table 2, isothermal crystallization results only in a minute increase in crystallinity as measured by WAXS, which agrees well with the observation of Cheng et al.[45] These authors showed that the increase in crystallinity with decreasing supercooling becomes less pronounced for low-crystallinity polypropylene.

While isothermal crystallization did not lead to any significant increase in percent crystallinity, the thermal history did affect the structure of the unit cell of the crystals for ePP and in particular the HI fraction, as well as the crystal sizes, as can be deduced from the analysis of the scattering plots shown in Figure 6. After isothermal crystallization, the crystalline peaks were shifted to higher *q* values, indicating a decrease in the unit cell dimensions (Table 3). This may be related to the reduced number of stereodefects within the crystalline lamellae. Our observations also agree with the observation of Cheng et al.[45] on the effect of decreasing

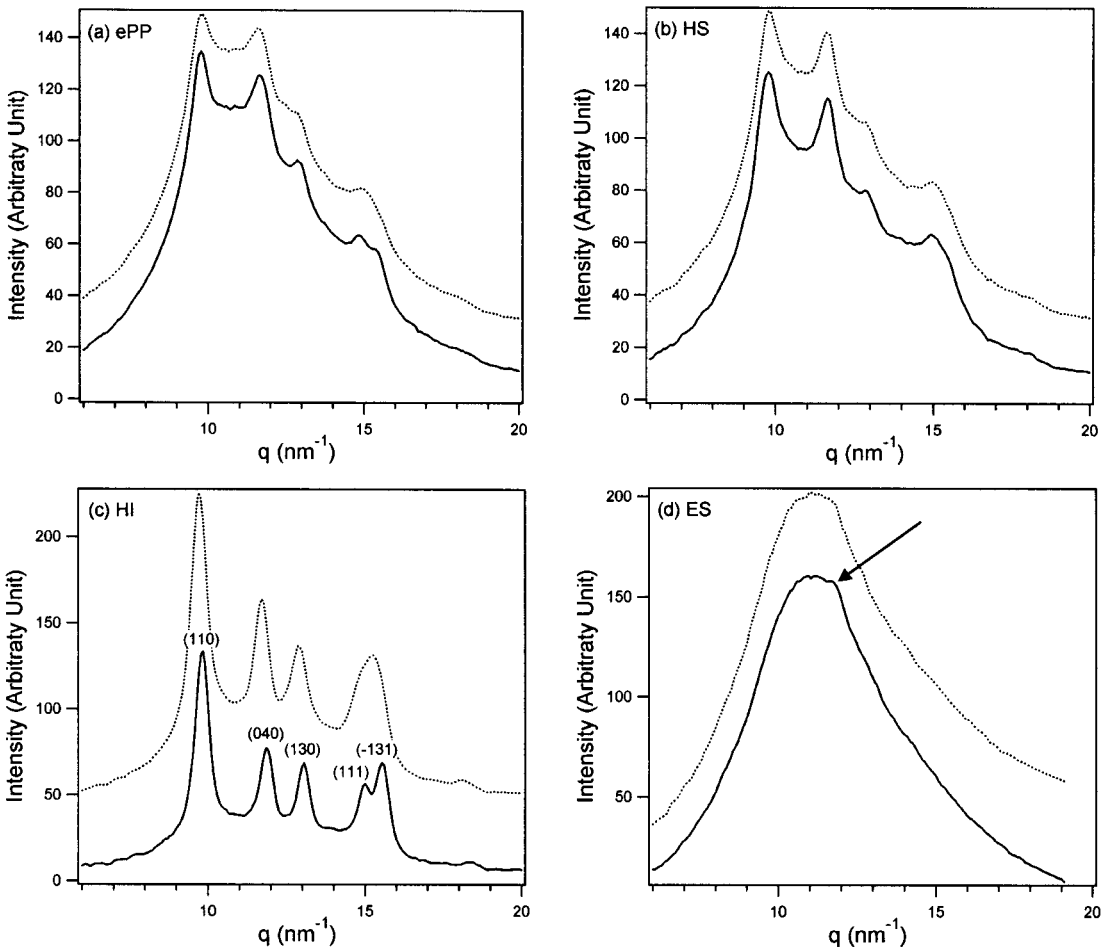

Figure 6. Plot of WAXS intensity profiles comparing isothermally (solid curves) and nonisothermally crystallized (dotted curves) materials of (a) unfractionated ePP, (b) HS fraction, (c) HI fraction, and (d) ES fraction. Crystalline peaks, as indicated for the HI fraction,[18] are reflections of α-phase iPP; the faint scattering peak for ES is indicated by an arrow. Curves are shifted along the *y*-axis for clarity.

supercooling on the unit cell dimensions of isotactic polypropylenes. In addition, after isothermal crystallization the single peak observed in the nonisothermal crystallized samples at around $q = 15.5$ nm^{-1} was split into two; thus, both (111) and (−131) reflections could be resolved. By comparing the peak width at half-maximum for e.g. the (110) reflections, the relative change in crystal size normal to the corresponding crystal plane for samples with different thermal histories could be assessed.[45,46] The unfractionated ePP and both the HS and HI fractions show an increase in crystal size for isothermally crystallized samples compared to nonisothermally crystallized samples. This observation is in full agreement with the work of Cheng et al. on isotactic polypropylene,[45] work by others on various polymers,[32,37] and polymer crystallization theory.[32,37] For the HI fraction the increase in crystal size normal to the (110) plane was estimated to be 10%, while for ePP and HS the increase was 15% and 12%, respectively.[47]

In Figure 7, the crystallinity data as determined by DSC for the various fractions crystallized at 120 °C are summarized together with the values derived from WAXS, AFM, and FT-IR spectroscopy. There is a good qualitative agreement among the results combined for all four methods. These results are further supported by the FT-IR data, which deviate not unexpectedly for the low-crystallinity ES fraction due to nonlinearities in the ratio of absorbances vs density curves.[34]

Despite its low crystallinity (8−11% as determined by WAXS and DSC), ePP can crystallize to form large hierarchical morphologies that are reminiscent of classical semicrystalline polymers. The nature of these morphologies depends on both the tacticity of the polymer and the thermal history, as revealed by investigations of the fractions of ePP. The nonisothermally crystallized ePP specimens also display the hierarchical ordering known from iPP,[18,20,21,35,37,38] including the presence of crosshatching of α-iPP.

The morphologies observed for the HI and HS fractions (Table 1) were similar (Figures 8 and 9, respectively). Spherulites and hedrites in various stages of development are evident. However, the nucleation density and perfection of these aggregates differed significantly for different fractions. While the HI fraction formed spherulitic entities (Figure 8), the HS fraction formed isolated large hedrites, very similar to the parent ePP (Figure 9). This qualitative difference in morphology may be attributed to a smaller fraction of crystallizable material in the HS fraction. In addition, the high degree of crystallinity in the HI fraction is reflected in the almost exclusive presence of bright lamellar features in the phase image shown in Figure 8 (right). Nonisothermal crystallization of the HI and HS fractions resulted in much less well-defined hedritic or spherulitic features, presumably due to the faster crystallization kinetics at lower temperatures during

Table 3. WAXS Data

sample	crystal plane	q_{max} (nm^{-1})	$d = 2\pi/q_{max}$ (nm)	peak width at half max height (1/nm)
HI	(110)	9.71	0.65	0.570
	(040)	11.72	0.54	
	(130)	12.93	0.49	
	(111), (−131)	15.27	0.41	
	a	18.22	0.34	
HI isothermal	(110)	9.85	0.64	0.516
	(040)	11.92	0.53	
	(130)	13.06	0.48	
	(111)	15.07	0.42	
	(−131)	15.61	0.40	
	a	18.55	0.34	
HS	(110)	9.85	0.64	0.711
	(040)	11.72	0.54	
	(130)	12.86	0.49	
	(111), (−131)	15.00	0.42	
HS isothermal	(110)	9.85	0.64	0.617
	(040)	11.72	0.54	
	(130)	12.93	0.49	
	(111), (−131)	15.00	0.42	
ePP	(110)	9.78	0.64	0.804
	(040)	11.72	0.54	
	(130)	13.06	0.48	
	(111), (−131)	15.27	0.41	
ePP isothermal	(110)	9.78	0.64	0.715
	(040)	11.79	0.53	
	(130)	13.06	0.48	
	(111)	14.94	0.42	
	(−131)	15.47	0.41	
	a	18.55	0.34	
ES	*a*	11.39	0.55	
ES isothermal	*a*	11.39	0.55	

[a] Scattering peaks cannot be assigned unambiguously; see text for details.

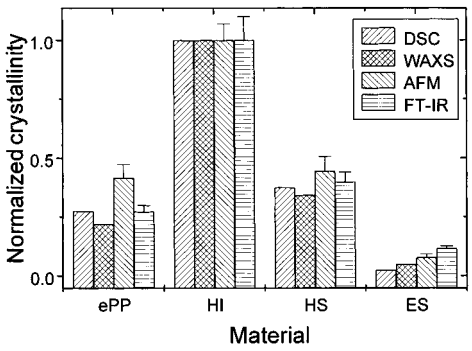

Figure 7. Crystallinities normalized to the crystallinity of HI for films crystallized isothermally at 120 °C as determined by various methods.[58]

cooling. However, rather well developed crosshatching was observed for both samples by TM-AFM.

The presence of hedrites and spherulites in isothermally crystallized films is further substantiated by optical microscopy. The isothermally crystallized HS specimen shows the presence of giant immature spherulites, whereas the nonisothermally crystallized HS sample shows only very small birefringent features (Figure 10). That these features are due to crystallites was confirmed by the absence of any transmitted light through the crossed polarizers above 125 °C.[48]

The ES fraction exhibits a markedly different morphology, which reflects the very low degree of crystallinity in this sample. Features observed in the TM-AFM images are usually short, often blocklike or curved, presumably due to the frequent imperfections and/or shorter isotactic sequences. More importantly, they do not show any ordered arrangements of higher hierarchical order, such as hedrites or spherulites. In addition, the crosshatched morphology typical for α-phase iPP was only occasionally observed. In Figure 11a, individual short lamellae in edge-on orientation can be recognized at the surface of the films. In some cases we observed crosshatched lamellae that developed at room temperature in nonisothermally crystallized samples (Figure 11b). A comparison of parts a and c of Figure 11 shows that the limited length and the presence of bundling are qualitatively more pronounced in the nonisothermally crystallized samples.

We have also employed an in situ hot stage TM-AFM[49] to determine the melting points of the lamellae seen for ES. We found that the lamellar features disappeared at temperatures between ca. 100 and 120 °C.[50] Despite the much lower heating rate used in the in situ AFM experiments compared to the DSC measurements, this temperature is significantly higher than any melting peak detected by DSC.

It is clear that each fraction shows distinctively different morphological details, but in general it can be concluded that images of the HS and HI fractions reveal morphologies typical for isothermally crystallized films of other polymers, i.e., lamellae, hedrites, and spherulites.[20,21,35,37] In contrast, the low-crystallinity ES fraction displays predominantly individual lamellae or "bundles" of lamellae. In most cases the lamellae were observed in edge-on orientation. Occasionally, we observed individual flat-on lamellae for the ES fraction (Figure 12). Crosshatching[39] was found in all fractions. The morphological features observed by TM-AFM provide good evidence for crystallinity in all fractions, including the lowest tacticity ES fraction, and thus agree with the DSC and WAXS data.

Discussion

In this work, we have shown that crystallization of low-tacticity elastomeric polypropylenes results in morphology that are reminiscent of highly crystalline thermoplastics. The beautiful two-dimensional spherulite observed by TM-AFM for a 200 nm thin film of isothermally crystallized ePP for instance spans ca. 200 μm (Figure 1).[36] These morphologies are representative of the bulk and are not just surface phenomena, as indicated by complementary studies using polarized optical microscopy (Figures 1 and 2 vs 4, Figures 9 vs 10).[51]

X-ray scattering experiments indicated that the ePP crystallizes in chain-folded crystals. The parent ePP material and the HS and HI fractions crystallize in the monoclinic α-modification of isotactic polypropylene (iPP), as shown by the WAXS data and supported by the observation of crosshatching. The WAXS data obtained for the ES fraction cannot be assigned unambiguously, while the presence of a small fraction of α-phase is evident from the AFM observation of occasional crosshatching.

The DSC endotherm scans show the presence of defined melting peaks. These transitions decrease in width and shift to higher temperatures when the samples were crystallized isothermally at 120 °C. For all samples two populations of melting peaks were observed. The low-temperature melting peaks around 40−50 °C can be ascribed to the melting of crystals that have crystallized during and after cooling to room

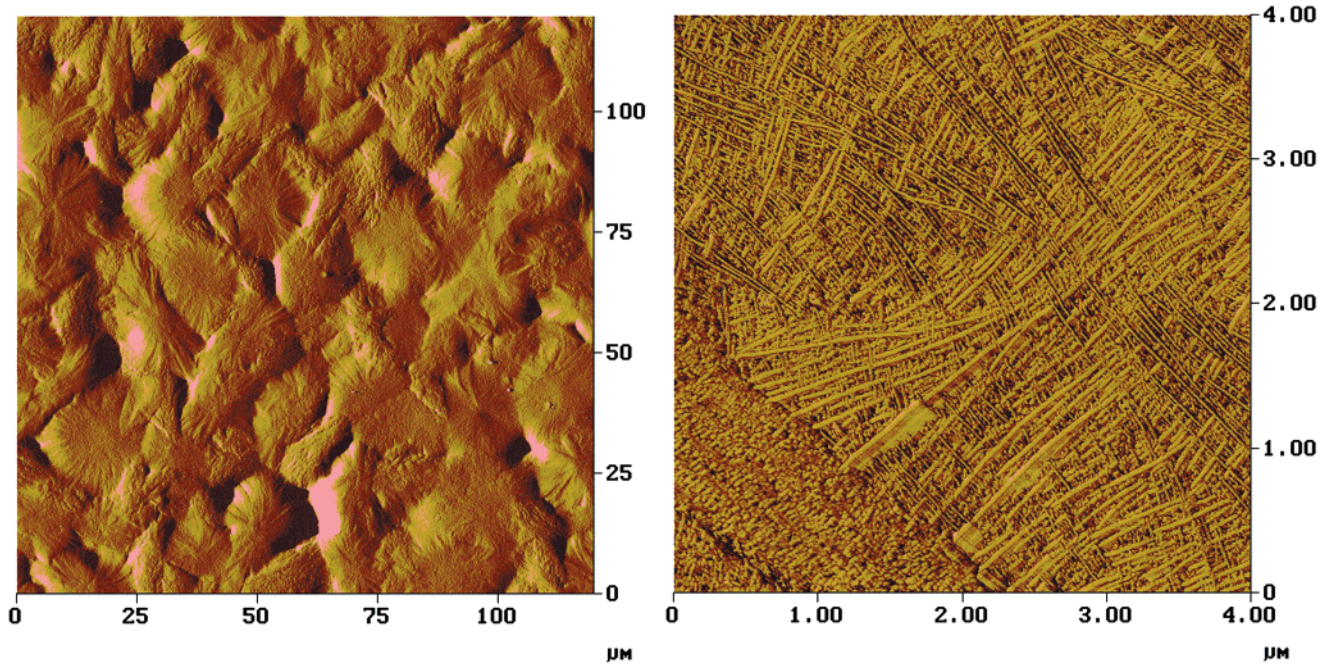

Figure 8. TM-AFM images of HI bulk film crystallized isothermally at 120 °C (left, amplitude image; right, phase image).[57]

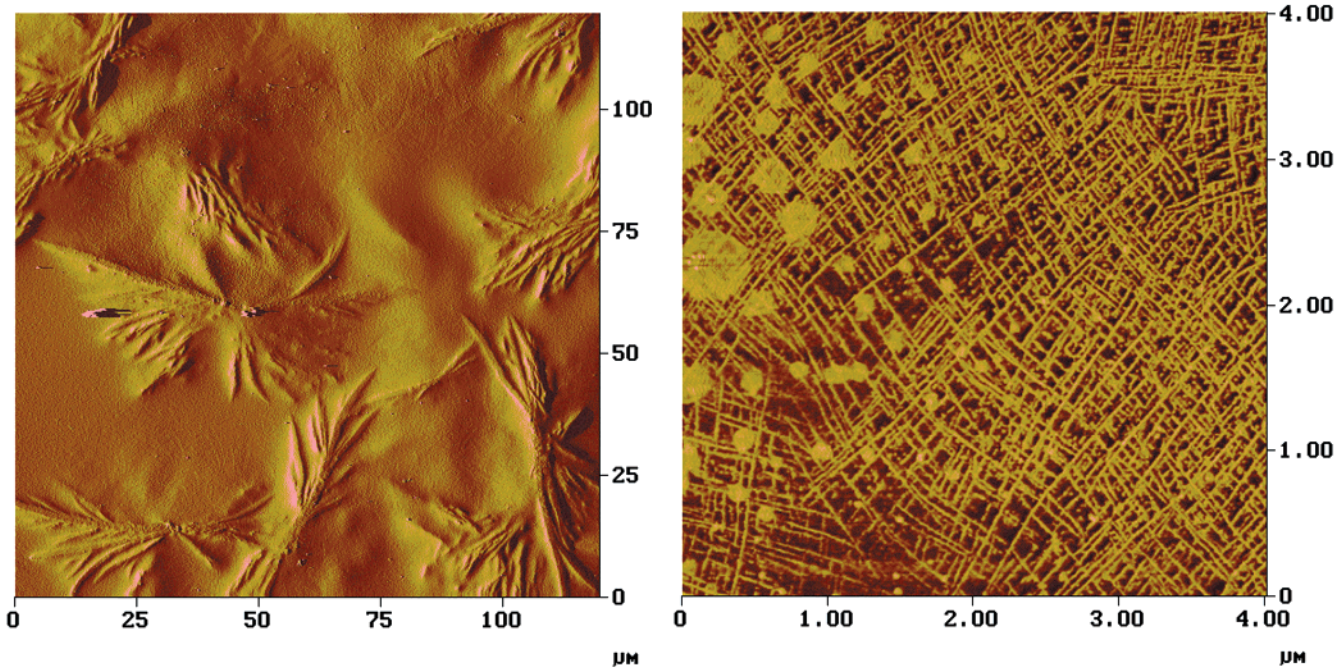

Figure 9. TM-AFM images of HS bulk film crystallized isothermally at 120 °C (left, amplitude image; right, phase image).[57]

temperature (secondary crystallization). The high-temperature melting peaks observed for ePP, HI, and faintly for HS correspond to crystals grown during cooling at high temperatures or during isothermal crystallization, depending on the experiment. For ePP and the HI fraction an additional peak or shoulder can be recognized in the high-temperature melting peaks.

The observation of multiple melting peaks for isothermally crystallized samples can be explained by the presence of two populations of crystallites.[32,52] The higher melting population of lamellae has grown at a high crystallization temperature under isothermal conditions. Crystallites with a lower melting point likely consist of material with less stereoregularity or shorter stereoregular sequences and have subsequently crystallized at lower temperature during and after rapid cooling of the sample. While the former fraction is characterized by presumably thicker and more perfect lamellae, the latter ones are significantly less perfect and may even contain chain ends and defects, i.e., short atactic sequences, within the interior of the lamellae. A final observation is that the DSC trace for the parent ePP material shows all the transitions present in the constituent fractions, which are in full agreement with previous work on similar materials.[12]

High-resolution TM-AFM images reveal structures most reasonably ascribed to edge-on lamellae. Evidence for these lamellae is observed even in the lowest crystallinity ES fraction (Figures 11 and 12). Several lines of evidence support our assignment of these

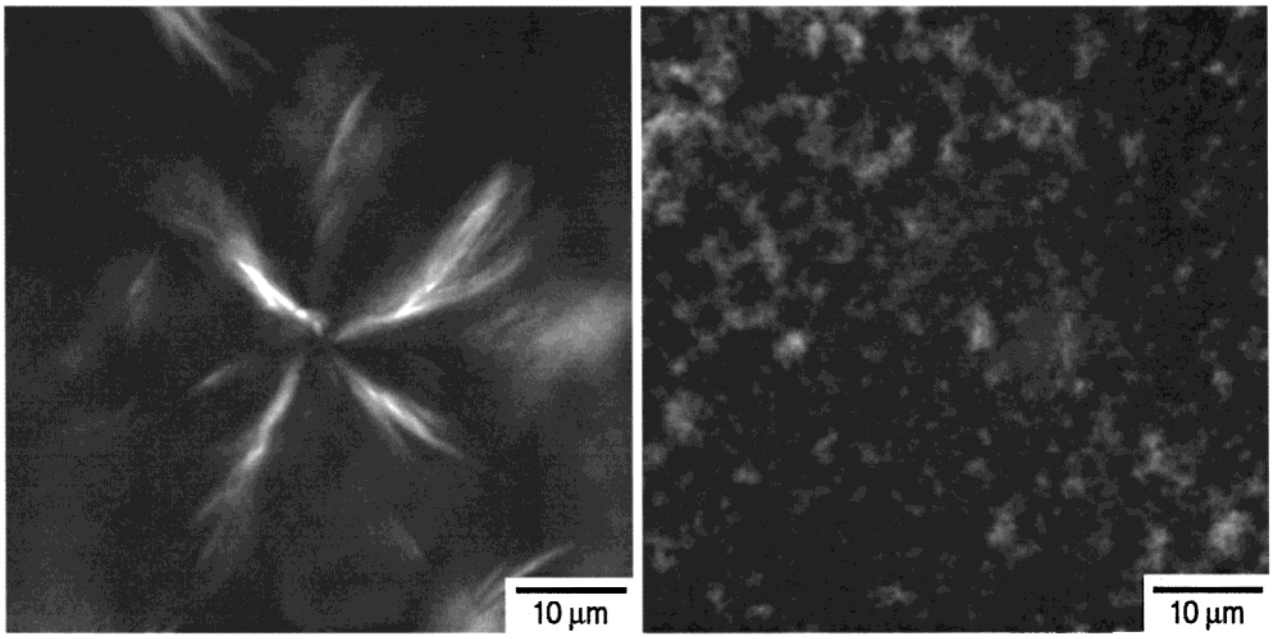

Figure 10. Optical micrographs obtained with crossed polarizers on HS films crystallized isothermally at 120 °C (left) and nonisothermally (right).

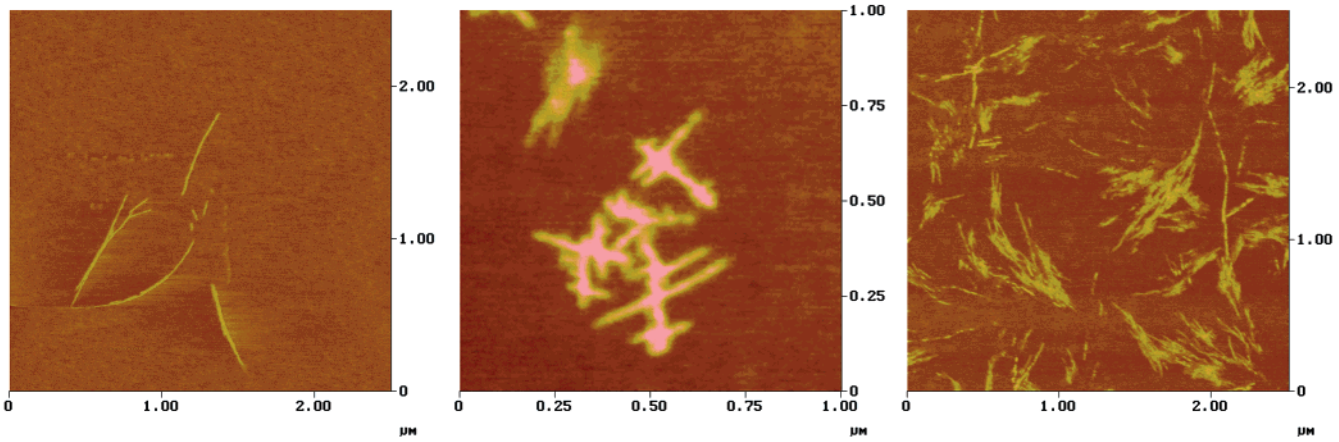

Figure 11. Comparison of TM-AFM phase images obtained at room temperature of (a) isothermally crystallized ES bulk film (T_c = 120 °C, left), (b) nonisothermally crystallized ES bulk film at an early stage (middle), and (c) nonisothermally (right) crystallized ES bulk film at a final stage.[57]

features as lamellae. The first is the crosshatched morphology for all samples (e.g., Figure 2b). The presence of defined angles of branching of 80° is, to within the error of the experiment, equal to the expected value for crosshatching for lamellae derived from the α-phase of isotactic PP. The width of these features (approximately 20−28 nm) is also consistent with that expected for polypropylene lamellae viewed in edge-on projection when the convolution due to the finite size of the AFM tip is taken into account (vide supra).

Furthermore, the similarity of the morphologies observed in these samples to the spherulitic and lamellar morphologies of other semicrystalline polymers[20,21,28,37,38] supports our assignment of these features to lamellae. The branching and splaying[37] of chain-folded lamellar crystals leads to spherulitic morphologies in other semicrystalline polymers. We may assume that the same mechanisms and processes and also chain folding occur in the ePP materials. In fact, the WAXS data agree very well with results obtained on chain-folded isotactic polypropylenes in the monoclinic α-modification.[18] A comparison of the DSC and WAXS data for nonisothermal and isothermal crystallization conditions also shows that the crystallites increase in perfection and size when crystallization is carried out at 120 °C. The thermal transitions occur at higher temperatures, and the melting peaks, as well as the WAXS scattering peaks (compare in particular the profiles for ePP and the HI fraction for both thermal histories in Figure 6a,c), sharpen compared to nonisothermally crystallized specimens. This behavior is typical for chain-folded lamellar crystals of polymers.[52] Finally, we occasionally observed flat polygonal-to-round objects in ES samples, which we interpret as flat-on chain-folded lamellae (Figure 12).[29,53] That the majority of the lamellae are in an edge-on orientation is consistent with reports that lamellae in polyolefins, and PP in particular, grow preferentially in edge-on orientation in thin films.[20,21,39,40,54]

The compositional heterogeneity of the elastomeric polypropylenes derived from 2-arylindenes has allowed us to investigate the morphologies of low-crystallinity polypropylenes as a function of tacticity and crystallin-

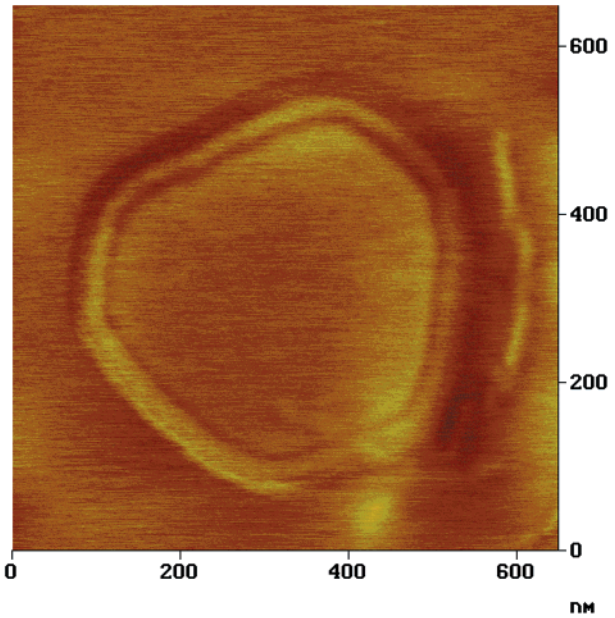

Figure 12. TM-AFM height image (z = 7 nm) of a flat-on lamella of ES grown isothermally at 120 °C for 2 h before quenching to room temperature. Because of the slow quenching, additional PP could crystallize which gives rise to the clearly discernible rim around the lamella.

ity. The molecular masses of the whole sample as well as the ES and HS fractions are similar (M_n from 87 000 to 95 000), while that of the HI fraction is higher at M_n = 172 000. The tacticities of these samples as measured by the percentage of isotactic pentads [mmmm] range from 21% for the ES fraction to 76% for the HI fraction. Investigation of these samples by all techniques employed has provided clear evidence for crystallinity in all fractions, including the lowest tacticity ES fraction. That the ES fraction possesses partial crystallinity is evident from the structures observed in the AFM images in Figures 11 and 12, and the fact that these structures disappear as the sample is heated to temperatures between 100 and 120 °C. Evidence for crystallinity in this sample was not conclusive from the DSC or X-ray data and estimated to be ±1% (Table 2), but at these very low levels of crystallinity, neither of these techniques can provide unambiguous evidence for crystallinity. AFM, on the other hand, is sensitive to the presence of morphological features, and hence crystallinity in a general sense, due to differences in local mechanical properties.[30] However, AFM is insensitive to the degree of disorder within the lamellae due to, for instance, incorporation of defects into the lamellae. Thus, at this level of magnification we can only indirectly extract quantitative information about the polymer crystals from the observation of the melting point of individual lamellae and the comparison with melting transitions of the other fractions.[48]

Our investigations of both ePP and its fractions have revealed several trends: the morphologies of these samples depend on both the tacticity of the samples and the thermal history. For ePP as well as the HI and HS fractions, isothermal crystallization at elevated temperatures (120−130 °C) yields large spherulitic or hedritic morphologies reminiscent of much more highly isotactic polypropylenes. These structures are less evident in samples that were cooled slowly (approximately 5 °C/min) from the melt (compare Figures 2 and 3b, Figures 4a vs 4b, Figures 10a vs 10b), indicating that crystallization kinetics play an important role in the evolution of these large hierarchical structures. Nevertheless, the high-resolution TM-AFM images give clear evidence for crosshatched lamellar structures for ePP, the HI fraction, and the HS fraction, irrespective of the crystallization conditions. This again indicates that AFM, while sensitive to the presence of morphological features, is insensitive to the degree of disorder within the lamellae due, for instance, to incorporation of atactic sequences or chain ends into the lamellae. DSC and WAXS, on the other hand, showed clearly that the perfection and size of the crystals increased when samples were crystallized isothermally at higher temperatures.

The observation of occasional crosshatching for the ES fraction (Figure 11b) is indirect evidence that the polymer chains possess a significant number of defects. These defects are most likely derived from atactic stereosequences that would be excluded from the chain-folded lamellae in isothermal crystallization at high temperatures but would be enriched near the interface between lamellae and amorphous phase. For ES, the density of defects seems to be close to a threshold that would still allow homoepitaxy (i.e., the growth of daughter lamellae on mother lamellae in crystallographically defined angles resulting in crosshatching) to occur. The density of the crosshatching varies systematically from ES (almost no crosshatching) to ePP to HS to HI (very dense crosshatching). This implies that the length of the stereoregular sequences increases, or the defect densities decrease, in the same order, a trend that is fully supported by the isotacticity [mmmm] estimated from ^{13}C NMR data. On the other hand, the rather high melting range of the ES crystals determined by in situ hot stage AFM (100−120 °C) suggests that the chain-folded lamellae are thermally quite stable and possess a significant degree of ordering. This observation demonstrates the usefulness of AFM in analyzing polymer phase transitions in situ since DSC showed no clear melting transition for the ES fraction and intensities related to the crystalline phase of PP in the WAXS data are low.

The observation of characteristic melting transitions, and the observation of lamellar morphology for all of the samples, including the lowest tacticity ES fraction, lead to the conclusion that all these materials crystallize. In addition, the WAXS intensities observed for all polymers, except for the ES fraction, are clearly related to the monoclinic α-phase of isotactic polypropylene. Thus, the chain-folded lamellar crystals are formed by predominantly stereoregular isotactic sequences. For the formation of lamellae, the length of the crystallizable segments must be at least of the order of a couple of fold lengths. Kravchenko et al.[13] presented an estimate of this block length derived from the classical method of HNO_3 treatment combined with GPC[55] and estimated a degree of polymerization of 118 for the isotactic stereosequences for a similar sample.

The elastomeric properties of these polypropylenes are due to the presence of stereodefects in the chains, which lower the crystallinity and provide amorphous sequences that can be oriented under application of a tensile strain. The distribution of these stereodefects has been the subject of considerable study,[12] but quantitative determinations of the length of isotactic and atactic stereosequences are difficult to establish since ^{13}C NMR

provides only average estimates of these quantities.[59] Attempts to infer information about the microstructure from the physical properties are compromised by the paucity of studies in the literature on the properties of random vs blocky polypropylenes. For ePP and its fractions, the observation of high melting crystallites in all fractions provides indirect evidence for long isotactic sequences; these long stereosequences could be reasonably ascribed to either a physical blend of isotactic polypropylene and lower tacticity polypropylenes or a stereoblock microstructure where the long crystallizable sequences coexist with atactic stereosequences in a given chain. The fact that these crystallites appear in fractions that are soluble in heptane or ether implies that these long isotactic sequences are chemically attached to amorphous sequences that solubilize the chains. Thus, the combination of the thermal and fractionation behavior coupled with studies by ^{13}C NMR[12,59] suggests that these materials are not a simple blend of isotactic and atactic polymer chains[56] but rather consist of polymer chains containing both isotactic and atactic stereosequences.[7,12,13,59]

Our results on the low-crystallinity polypropylenes can be compared to the elegant work of Bensason et al. on analogous polyethylene elastomers.[15] These authors were able to correlate the physical properties of low-density polyethylenes with their morphologies, which were in turn correlated to the amount of comonomer, density, and crystallinity in the ethylene copolymers.[15] At high crystallinities, spherulitic morphologies were observed, and at intermediate crystallinities the polyethylenes adopted a stacked lamellar morphology. For polyethylenes with densities less than 0.89 g/cm^3 a granular morphology was observed, which was proposed to be made up of bundled crystals or fringed micelles. The transition from lamellar morphologies to the granular "fringed micelles" coincided with the onset of elastomeric properties.

The low-crystallinity polypropylenes described in this work have similar densities and mechanical properties to the polyethylenes investigated by Bensason et al.[15] Despite the similarity in densities, degree of crystallinity, and physical properties, the morphology of the polypropylenes is markedly different. We see no clear evidence for "fringed-micelle"-type structures at lower crystallinities but rather observe lamellar morphologies even for the lowest crystallinity ES samples. The unfractionated ePP exhibits a morphology very similar to iPP. The appearance of a "fringed micellar" morphology and the presence of elastomeric properties are not directly linked in this case. For the polypropylenes, the lamellar morphologies observed for the HS and ES fractions indicate that long crystallizable isotactic sequences remain even in the lowest crystallinity samples. As a consequence of this blocky microstructure, lamellar crystals can still form even when the overall percentage of crystallizable material is low.

Conclusions

We have shown by a combination of techniques that elastomeric polypropylene (ePP) with a density of 0.86 g/cm^3 crystallizes from the melt into well-defined morphologies. We presented solid evidence that this class of materials, when crystallized isothermally from the melt, exhibits morphologies that are reminiscent of classical semicrystalline polymers. The presence of lamellae, crosshatching, hedrites, and spherulites was revealed by high-resolution tapping mode AFM and polarized optical microscopy. The findings reported herein show that a correlation among density, melting point, and morphology observed for the low-crystallinity polyethylenes is not readily extended to ePP. The presence of high-melting crystallites in low-density polymer fractions soluble in heptane and ether provides good evidence for a blocklike structure consisting of isotactic and atactic stereosequences. Our findings have direct consequences for the interpretation of the mechanical behavior of these and very likely other low-density polyolefin elastomeric materials. Fringed micelles are not necessarily required to observe elastomeric behavior. Current work in our groups addresses the morphology of other low-density polyolefins, the in situ study of crystallization, and the quantitative assessment of changes in molecular and lamellar orientation during tensile test experiments. This work will allow us to develop a general model that describes the impact of the thermal history on morphology and on the corresponding materials' mechanical properties.

Acknowledgment. H.S. gratefully acknowledges financial support by the Deutsche Akademischer Austauschdienst (DAAD) in the framework of the "Hochschulsonderprogramm III" and the NSF MRSEC Center on Polymer Interfaces and Macromolecular Assemblies (CPIMA) under DMR 9808677. G.G.F. and R.M.W. acknowledge support from the National Science Foundation (DMR-9910386). W.W. and J.A.P. acknowledge the support of the Stanford Synchrotron Radiation Laboratory in providing facilities used in these experiments: this work was supported by Department of Energy Contract DE-AC03-76SF00515.

References and Notes

(1) (a) Brintzinger, H. H.; Fischer, D.; Mülhaupt, R.; Rieger, B.; Waymouth, R. M. *Angew. Chem., Int. Ed. Engl.* **1995**, *34*, 1143. (b) *Metallocene-Based Polyolefins*; Scheirs, J., Kaminsky, W., Eds.; Wiley: Chichester, 2000; Vol. 1-2.

(2) (a) Ovitt, T. M.; Coates, G. W. *J. Am. Chem. Soc.* **1999**, *121*, 4072. (b) Tian, J.; Coates, G. W. *Angew. Chem., Int. Ed.* **2000**, *39*, 3626.

(3) (a) Deming, T. J. *Nature (London)* **1997**, *390*, 386. (b) Deming, T. J. *J. Polym. Sci., Part A: Polym. Chem.* **2000**, *38*, 3011.

(4) (a) Matyjaszewski, K.; Gaynor, S.; Greszta, D.; Mardare, D.; Shigemoto, T. *J. Phys. Org. Chem.* **1995**, *8*, 306. (b) Queffelec, J.; Gaynor, S. G.; Matyjaszewski, K. *Macromolecules* **2000**, *33*, 8629.

(5) Benoit, D.; Chaplinski, V.; Braslau, R.; Hawker, C. J. *J. Am. Chem. Soc.* **1999**, *121*, 3904.

(6) (a) Yu, S. J. M.; Conticello, V. P.; Zhang, G. H.; Kayser, C.; Fournier, M. J.; Mason, T. L.; Tirrell, D. A. *Nature (London)* **1997**, *389*, 167. (b) Krejchi, M. T.; Atkins, E. D. T.; Waddon, A. J.; Fournier, M. J.; Mason, T. L.; Tirrell, D. A. *Science* **1994**, *265*, 1427.

(7) Natta, G. *J. Polym. Sci.* **1959**, *34*, 531.

(8) (a) Collette, J. W.; Ovenall, D. W.; Buck, W. H.; Ferguson, R. C. *Macromolecules* **1989**, *22*, 3858. (b) Collette, J. W.; Tullock, C. W.; MacDonald, R. N.; Buck, W. H.; Su, A. C. L.; Harrel, J. R.; Mülhaupt, R.; Anderson, B. C. *Macromolecules* **1989**, *22*, 3851. (c) Job, R. C. U.S. Patent 5,089,573, 1992. (d) Ittel, S. D. *J. Macromol. Sci., Chem.* **1990**, *A27*, 9.

(9) (a) Mallin, D. T.; Rausch, M. D.; Lin, Y. G.; Dong, S.; Chien, J. C. W. *J. Am. Chem. Soc.* **1990**, *112*, 2030. (b) Bravakis, A. M.; Bailey, L. E.; Pigeon, M.; Collins, S. *Macromolecules* **1998**, *31*, 1000. (c) Dietrich, U.; Hackmann, M.; Rieger, B.; Klinga, M.; Leskelae, M. *J. Am. Chem. Soc.* **1999**, *121*, 4348. (d) Dreier, T.; Erker, G.; Frohlich, R.; Wibbeling, B. *Organometallics* **2000**, *19*, 4095.

(10) (a) Coates, G. W.; Waymouth, R. M. *Science* **1995**, 217. (b) Bruce, M. D.; Coates, G. W.; Hauptman, E.; Waymouth, R. M.; Ziller, J. W. *J. Am. Chem. Soc.* **1997**, *119*, 11174.

(11) Gauthier, W. J.; Corrigan, J. F.; Taylor, N. J.; Collins, S. *Macromolecules* **1995**, *28*, 3771.
(12) (a) Carlson, E. D.; Krejchi, M. T.; Shah, C. D.; Terekawa, T.; Waymouth, R. M.; Fuller, G. G. *Macromolecules* **1998**, *31*, 5343. (b) Hu, Y.; Carlson, E. D.; Waymouth, R. M.; Fuller, G. G. *Macromolecules* **1999**, *32*, 3334. (c) Kravchenko, R.; Masood, A.; Waymouth, R. M.; Myers, C. L. *J. Am. Chem. Soc.* **1998**, *120*, 2039. (d) Carlson, E. D.; Fuller, G. G.; Waymouth, R. M. *Macromolecules* **1999**, *32*, 8094.
(13) Kravchenko, R. L.; Sauer, B. B.; McLean, R. S.; Keating, M. Y.; Cotts, P. M.; Kim, Y. H. *Macromolecules* **2000**, *33*, 11.
(14) Ho, T.; Martin, J. M. In *Metallocene-Based Polyolefins*; Scheirs, J., Kaminsky, W., Eds.; Wiley: Chichester, 2000; Vol. 2, p 175.
(15) Bensason, S.; Minick, J.; Moet, A.; Chum, S.; Hiltner, A.; Baer, E. *J. Polym. Sci., Part B: Polym. Phys.* **1996**, *34*, 1301.
(16) *Thermoplastic Elastomers*; Holden, G., Legge, N. R., Quirk, R. P., Schroeder, H. E., Eds.; Hanser Publishers: New York, 1996.
(17) The materials described in ref 12 were synthesized with a zirconocene catalyst system which leads to a polymer with slightly different characteristics, whereas here we discuss materials derived from a hafnium catalyst.
(18) Vancso, G. J. In *Polypropylene: An A−Z Reference*; Karger-Kocsis, J., Ed.; Kluwer Academic: Dordrecht, 1999; p 510.
(19) Numerous polymorphic forms of iPP are known: Natta, G.; Corradini, P.; Cesari, M. *Rend. Atti Acc. Naz. Lincei* **1956**, *21*, 365. (b) Keith, H. D.; Padden Jr., F. J.; et al. *J. Appl. Phys.* **1959**, *30*, 1485. (c) Turner-Jones, A.; et al. *Makromol. Chem.* **1964**, *75*, 134. (d) Bruckner, S.; Meille, S. V.; Petraccone, V.; Pirozzi, B. *Prog. Polym. Sci.* **1991**, *16*, 361. (e) Auriemma, F.; deBallesteros, O. R.; DeRosa, C.; Corradini, P. *Macromolecules* **2000**, *33*, 8764 and cited references. (f) Phillips, R. A.; Wolkowicz, M. D. In *Polypropylene Handbook*; Moore, Jr., E. P., Ed.; Hanser Publishers: Munich, 1996.
(20) For a morphological study by AFM on α-iPP, see: Schönherr, H.; Snétivy, D.; Vancso, G. J. *Polym. Bull. (Berlin)* **1993**, *30*, 567.
(21) For morphological studies by AFM on *β*-iPP, see: Trifonova-van Haeringen, D.; Varga, J.; Ehrenstein, G. W.; Vancso, G. J. *J. Polym. Sci., Part B: Polym. Phys.* **2000**, *38*, 672.
(22) High-resolution AFM has revealed details of the molecular structure of the different modifications of iPP. See: (a) Stocker, W.; Magonov, S. N.; Cantow, H. J.; Wittmann, J. C.; Lotz, B. *Macromolecules* **1993**, *26*, 5915. (b) Snétivy, D.; Guillet, J. E.; Vancso, G. J. *Polymer* **1993**, *34*, 429. (c) Stocker, W.; Schuhmacher, M.; Graff, S.; Thierry, A.; Wittmann, J. C.; Lotz, B. *Macromolecules* **1998**, *31*, 807 and cited references.
(23) Wiyatno, W.; Waymouth, R. M.; Fuller, G. G.; et al. Manuscript in preparation.
(24) Waymouth, R. M.; Chen. Z. R.; et al. Manuscript in preparation.
(25) Isotactic polypropylene melts at ca. 165 °C.[43b]
(26) The characterization of (ultra)thin films of ePP and their crystallization behavior will be reported in a separate paper: Schönherr, H.; Waymouth, R. M.; Frank, C. W.; et al. Manuscript in preparation.
(27) Due to heat generated by the AFM, this corresponds to a true sample temperature of ca. 34 °C.
(28) For reviews of AFM studies on polymers, see: (a) Goh, M. C. In *Advances in Chemical Physics*; Prigogine, I., Rice, S. A., Eds.; Wiley & Sons: New York, 1995; Vol. XCI. (b) *Scanning Probe Microscopies in Polymer*s; Ratner, B. D., Tsukruk, V., Eds.; *ACS Symp. Ser.* **1998**, *694*. (c) *Microstructure and Microtribology of Polymer Surfaces*; Tsukruk, V., Wahl, K. J., Eds.; *ACS Symp. Ser.* **1999**, *741*.
(29) Schönherr, H.; Waymouth, R. M.; Hawker, C. J.; Frank, C. W. *ACS Polym. Mater.: Sci. Eng.* **2001**, *84*, 453.
(30) Magonov, S. N.; Elings, V.; Whangbo, M.-H. *Surf. Sci.* **1997**, *372*, L385.
(31) The set point ratio was varied between 0.4 and 0.9 with no apparent change in relative contrast; i.e., the amorphous matrix always showed a phase lag relative to the crystallites and lamellae. For a discussion of image contrast and its dependence on scanning conditions, see e.g.: (a) Reference 30. (b) Bar, G.; Thomann, Y.; Brandsch, R.; Cantow, H.-J.; Whangbo, M.-H. *Langmuir* **1997**, *13*, 3807.
(32) Wunderlich, B. *Macromolecular Physics*; Academic Press: New York, 1976; Vol. 2.
(33) Sundell, T.; Fageholm, H.; Crozier, H. *Polymer* **1996**, *37*, 3227.
(34) Hobbs, J. P.; Sung, C. S. P.; Krishnan, K.; Hill, S. *Macromolecules* **1983**, *16*, 193 and cited references.
(35) (a) Keller, A. In *Growth and Perfection of Crystals;* Doremus, R. H., Roberts, B. W., Turnbull, D., Eds.; Wiley: New York, 1958; pp 499−532. (b) Norton, D. R.; Keller, A. *Polymer* **1985**, *26*, 704.
(36) With a diameter of ca. 200 μm this 2-D spherulite exceeds the maximum scan range available.
(37) Bassett, D. C. *Principles of Polymer Morphology*; Cambridge University Press: Cambridge, 1981. (b) Bassett, D. C. *Macromol. Symp.* **1999**, *143*, 11.
(38) Geil, P. H. *Polymer Single Crystals*; Wiley-Interscience: New York, 1963; Chapter 3.
(39) (a) Khoury, F. *J. Res. Natl. Bur. Stand.* **1966**, *70A*, 29. (b) Padden, F. J.; Keith, H. D. *J. Appl. Phys.* **1966**, *37*, 4013. (c) Lotz, B.; Wittmann, J. C. *J. Polym. Sci., Polym. Phys.* **1986**, *24*, 1541.
(40) (a) Bassett, D. C.; Olley, R. H. *Polymer* **1984**, *25*, 935. (b) Olley, R. H.; Bassett, D. C. *Polymer* **1989**, *30*, 399.
(41) Silicon grating GT01, Mikromasch, Tallinn, Estonia.
(42) Lamellar thicknesses of 13−17 nm were reported for crystallization temperatures of 120 and 130 °C. See: (a) Ceres, B. V.; Schultz, J. M. *J. Appl. Polym. Sci.* **1984**, *29*, 4183. Further data can be found in: (b) Mezghani, K.; Campbell, R. A.; Philips, P. J. *Macromolecules* **1994**, *27*, 997.
(43) (a) Samuels, R. J.; Yee, R. Y. *J. Polym. Sci., Part A2* **1972**, *10*, 385. (b) Karger-Kocsis, J. *Polypropylene: Structure, Blends and Composites*; Chapman & Hall: New York, 1995.
(44) Atactic polypropylene was synthesized with a bis(2-phenylindenyl)hafnium dichloride catalyst at 75 psi and 20 °C. GPC analysis showed $M_w = 375$ kg/mol and $M_w/M_n = 2.2$, and ^{13}C NMR showed an average pentad distribution [mmmm] = 9% (ref 10b).
(45) Cheng, S. Z. D.; Janimak, J. J.; Zhang, A. Q.; Hsieh, E. T. *Polymer* **1991**, *32*, 648.
(46) (a) Scherrer, P. *Nachr. Ges. Wiss. Göttingen* **1918**, 98; in *Kolloidchemie*; Zsigmondy, R., Ed.; Spamer: Leipzig, 1920. (b) Baltá-Calleja, F. J.; Vonk, C. G. *X-ray Scattering of Synthetic Polymers*; Elsevier: New York, 1989.
(47) A quantification of the lamellar thicknesses using small-angle X-ray scattering (SAXS)[45] was not attempted in the present study.
(48) The fractions showed the following melting points as determined by POM (disappearance of birefringence): ePP, 145 °C; HI, 168 °C; HS, 125 °C; ES, not detectable due to absence of birefringence.
(49) (a) Pearce, R.; Vancso, G. J. *Macromolecules* **1997**, *30*, 5843. (b) Schultz, J. M.; Miles, M. J. *J. Polym. Sci., Part B: Polym. Phys.* **1998**, *36*, 2311.
(50) The temperature was increased in increments of ca. 5 °C. After stabilization of the imaging conditions usually two images were acquired within 8 min. Since we have used AFM unheated cantilevers, heat transfer from sample to the tip−cantilever assembly reduces the actual sample surface temperature. This leads to an uncertainty of the true sample surface temperature of several °C (Schönherr, H.; Bailey, L. E.; Frank, C. W. *Langmuir* **2001**, *17*, in press).
(51) These film samples with film thicknesses of several micrometers to millimeters are considered representative of the bulk. In fact, most of the classic morphological work on semicrystalline polymers was and is carried out on such film samples by means of polarized OM.
(52) Gedde, U. *Polymer Physics*, 1st ed.; Kluwer Academic Publishers: Dordrecht, 1995.
(53) Nisman, R.; Smith, P. F.; Vancso, G. J. *Langmuir* **1994**, *10*, 1667.
(54) The crystallization of the ES fraction can also be followed in real time by in situ hot stage TM-AFM (Schönherr, H.; Frank, C. W.; Waymouth, R. M., unpublished data). The growth of lamellae from the initially observed cigar-shaped features proceeds almost exclusively in one direction while the width of the lamellae does not change. The growth thus resembles the lamellar growth observed by various authors using this technique (refs 29 and 49).
(55) Williams, T.; Blundell, D. J.; Keller, A.; Ward, I. M. *J. Polym. Sci., Part A-2* **1968**, *6*, 1613.
(56) It has been shown by Keith and Padden that isotactic polypropylene can crystallize as a minor component in a 10:90 mixture with atactic polypropylene: Keith, H. D.; Padden, F. J. *J. Appl. Phys.* **1964**, *35*, 1270.

(57) TM-AFM amplitude and phase images are presented without absolute color scale. Since the magnitude of both signals is affected by various scan parameters, such as the precise amplitude of the free vibrating cantilever, the set point ratio,[30, 31] the gains of the feedback loop, etc., the values given by the AFM software can only be considered as relative values.

(58) The error bars correspond to the error calculated by Gauss error analysis with 2sd from multiple independent experiments as error in the individual crystallinity.

(59) Busico, V.; Cipullo, R.; Segre, A. L.; Talarico, G.; Vacatello, M.; Castelli, V. V. A. *Macromolecules* **2001**, *34*, 8412.

MA010959M